Symmetry of zinc oxide nanostructures

2006 J. Phys.: Condens. Matter 18 1939

(http://iopscience.iop.org/0953-8984/18/6/010)

INSTITUTE OF PHYSICS PUBLISHING JOURNAL OF PHYSICS: CONDENSED MATTER

J. Phys.: Condens. Matter **18** (2006) 1939–1953 doi:10.1088/0953-8984/18/6/010

Symmetry of zinc oxide nanostructures

Ivanka Milošević[1], Vladan Stevanović[1], Pierre Tronc[2] and Milan Damnjanović[1]

[1] Faculty of Physics, University of Belgrade, POB 368, 11001 Belgrade, Serbia[3]
[2] Laboratoire d'Optique Physique, Ecole Supérieure de Physique et Chimie Industrielles, 10 rue Vauquelin, 75005 Paris, France

E-mail: ivag@afrodita.rcub.bg.ac.yu

Received 15 September 2005, in final form 4 January 2006
Published 24 January 2006
Online at stacks.iop.org/JPhysCM/18/1939

Abstract

The full geometrical symmetry groups of zinc oxide nanowires, nanotubes, nanosprings and nanorings are found and some physical properties which can be deduced from the symmetry are discussed: conserved quantum numbers and band degeneracies; dynamical representations, Raman and infrared active modes; piezoelectric tensor.

1. Introduction

Since the discovery of the functional semiconducting oxide nanostructures [1] diverse nanosized forms of zinc oxide have been synthesized (for a review see, e.g., [2]). In addition to the unique combination of semiconducting and piezoelectric properties of the bulk, a nanostructured ZnO single crystal exhibits quite novel electro-optical and mechanical properties. Being also bio-safe and bio-compatible it shows good potential to take the role of a key nanotechnological material in future research and applications.

Although there is a vast number of papers on growth techniques of ZnO nanostructures [2], and reports on experimental research of their Raman spectra [3] and optical properties [4, 5], photoluminescence [6] in particular, there is an apparent lack of theoretical investigations of these structures. In this paper we analyse the structure and symmetry of ZnO nanowires (nanorods), nanotubes, seamless nanorings, nanosprings (nanohelices) and superlattice structured nanohelices [7] and discuss their symmetry based properties. The results presented can be helpful in experimental data analysis and in further quantitative estimations of the physical properties of these technologically interesting materials. Namely, symmetry based considerations proved to be extremely fruitful in a context of the carbon nanotubes [8, 9] and without doubt will be an indispensable tool in studying the diversity of ZnO nanostructures.

In section 2 we study a variety of the nanostructures and describe their symmetry in terms of the line groups [9–11, 19]. For each of these structures we give the orbit types and the site

[3] http://www.ff.bg.ac.yu/nanoscience

symmetry groups (stabilizers), i.e. we specify the asymmetric cell (also called the full symmetry cell or symcell). For the translationally periodic structures with crystallographic principal axes, the corresponding line groups are in the physics of semiconductors known as the rod groups, and we give the rod-group notation [12] as well. Section 3 is devoted to direct consequences of the found symmetry. Some of them are quite general (e.g. conserved quantum numbers and band degeneracy). On the other hand, classification of Raman active modes is motivated by the great importance of Raman spectroscopy in characterizing carbon and inorganic nanotubes, while the piezoelectricity is singled out as one of the most significant ZnO characteristics.

2. Symmetry

Zinc oxide, the mineral zincite, crystallizes in the wurtzite structure whose underlying Bravais lattice is hexagonal (space group $P6_3mc = C_{6v}^4$). The lattice parameters are $b = b_1 = b_2 = 3.25$ Å (in the xy-plane), $b_3 = 5.21$ Å (along the z-axis) and the structure is characterized by tetrahedral coordination of the ion of one kind (e.g. Zn^{2+}) by the ions of the other kind (O^{2-}). Therefore, as the isogonal point group of the zincite does not contain an inversion, the crystal is a piezoelectric.

2.1. Nanowires and nanotubes

Over past few years a variety of techniques (e.g. the catalysed vapour–liquid–solid process [13], vapour phase growth on large area substrates [14], metal-catalyst-free [15] and plasma-assisted molecular beam epitaxy [16]) have been used to synthesize ZnO nanowires and nanotubes. Quite recently, controlled synthesis of these nanostructures has been reported [17]. The as-produced nanowires and nanotubes have been characterized and analysed by means of scanning electron microscopy, x-ray diffraction, transmission electron microscopy, selected area electron diffraction, and energy dispersive spectrometry. They are shown to retain the hexagonal symmetry of the bulk. Some of the growth techniques [18] lead to the formation of single-crystal ZnO nanotubes. Typically, the length of the nanowires and nanotubes ranges from 100 μm to 1 mm while the diameter varies from 50 to 500 nm.

ZnO nanowires can be imagined as hexagonal rods sawn from the bulk along planes parallel to the symmetry axes, retaining thus the z-periodicity of the bulk. However, the wurtzite structure has two types of the rotational axes along the z-direction: a third-order rotational axis C_3 which runs through the atoms, and a sixth-order screw axis, generated by $(C_6|b_3/2)$, which goes through the centres of hexagons formed by the atoms. Therefore, in principle, two types of nanowires (and nanotubes) can be obtained.

The structures of the first type (3xH and 3yH structures) are obtained in the following way. By sawing regular hexagons around the pure rotational axis (at the distance $n_2 b\sqrt{3}/2$) along the planes perpendicular to $\boldsymbol{e}_x = \boldsymbol{b}_1 + 2\boldsymbol{b}_2$ and with the vectors successively rotated by $\pi/3$, the 3xH structure is obtained. If the hollow is made by cutting out a coaxial rod at the distance $n_1 b\sqrt{3}/2$ ($0 \leqslant n_1 < n_2$) (figure 1) a nanotube, parameterized as (n_1, n_2), is obtained. Hence, the wall thickness is given by $(n_2 - n_1)b\sqrt{3}/2$ and the nanowire can be seen as a $(0, n_2)$ 'nanotube'.

When cutting the bulk along the planes perpendicular to $\boldsymbol{e}_y = \boldsymbol{b}_1$ (and rotated directions) one gets nanowires and nanotubes of the type 3yH, figure 1. The wall thickness of a nanotube is given by $(n_2 - n_1)b/2$, while $n_2 b$ is the diameter of a nanowire (or the outer diameter of a nanotube).

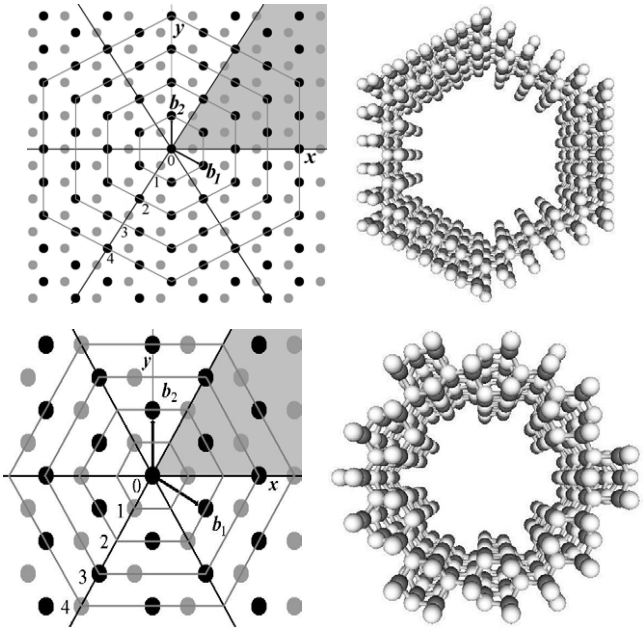

Figure 1. Nanotubes of the 3H type. Left panels: top view of the bulk. Points denote zinc atoms at $z = 0$ (the black ones) and at $z = b_3/2$ (the grey ones). Lines depict positions of the vertical mirror planes. The third-order rotational axis is in their intersection. The symmetry cell is shaded. Right panels: 3xH (3, 5) and 3yH(3, 6) nanotubes.

The symmetry group of both structures is the line group [19]:

$$\boldsymbol{L}_{3\mathrm{H}} = \boldsymbol{T}(b_3)\boldsymbol{C}_{3\mathrm{v}}, \tag{1}$$

where $\boldsymbol{T}(b_3)$ is the translational group with period b_3 and $\boldsymbol{C}_{3\mathrm{v}}$ is the point group generated by rotations of $2\pi/3$ and reflections in the vertical mirror plane. As this is a translationally periodic structure, with crystallographic principal axes, $\boldsymbol{L}_{3\mathrm{H}}$ is the rod group [12] No 49, with the international symbol $\boldsymbol{p}3\boldsymbol{m}1$. Hence, the symmetry does not depend on the (n_1, n_2) parameters, unlike the case of carbon nanotubes [9].

The type I nanotubes consist of two different orbital types [19, 11] (the set of atoms generated from one of them by the group transformations): a_1 type (having trivial stabilizer) and b_1 type (being invariant under vertical mirror reflections), while the nanowires have an additional orbit of the d_1 type whose stabilizer is the isogonal point group $\boldsymbol{C}_{3\mathrm{v}}$, as the atoms sit in the nanowire axis retaining the site symmetry of the bulk. The structures 3xH and 3yH, however, differ in the number of orbits they are built of (see table 1).

Analogously, by sawing around the screw axis one gets the hexagonal structures 6xH and 6yH, figure 2. However, in the 6xH case the sawing planes are closely stacked. Their distance is $b\sqrt{3}/6$. (Note that the first plane and those at the distance $nb\sqrt{3}/2$ do not contain atoms and should not be considered, therefore.)

Thus, the 6H structures are characterized by (n_1, n_2), with integers n_1 and n_2 (being not divisible by three in the 6H structures) and $1 < n_1 < n_2$. The symmetry of both the structures is described by the rod group No 70 ($\boldsymbol{p}6_3\boldsymbol{mc}$) [12], being the non-symmorphic line group [19] (independently of n_1 and n_2):

$$\boldsymbol{L}_{6\mathrm{H}} = \boldsymbol{T}_6^1(b_3)\boldsymbol{C}_{3\mathrm{v}}, \tag{2}$$

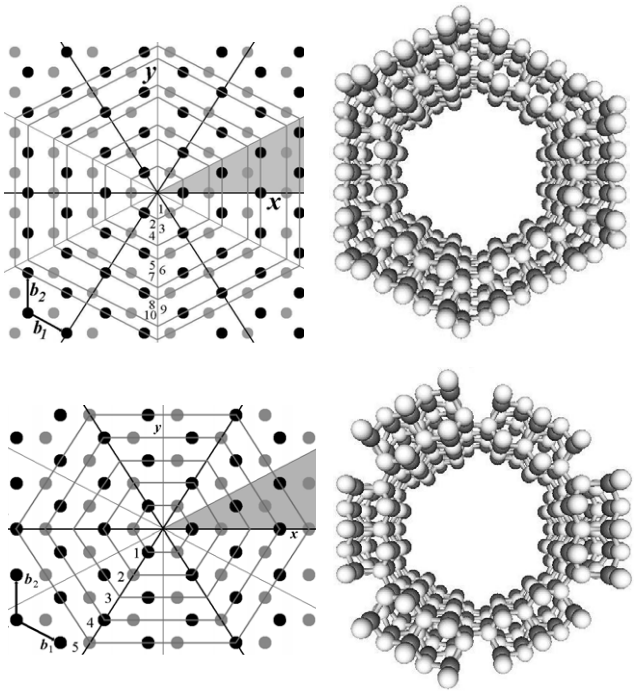

Figure 2. Nanotubes of the 6H type. Left panels: top view of the bulk. The walls are enumerated. Points denote zinc atoms at $z = 0$ (the black ones) and at $z = b_3/2$ (the grey ones). Mirror and glide planes are indicated by thick and thin lines, respectively. The sixth-order screw axis is in their intersection. The symmetry cell is shaded. Right panels: 6xH (6, 12) and 6yH(3, 6) nanotubes.

Table 1. Nanowire and nanotube orbit decomposition. For the nanostructure (NS) specified in the first column, the line group family (LGF), the orbit types (according to [19], column OT, and the corresponding Wyckoff letter, column W), the corresponding site symmetries (SITE) in two notations, and the total numbers $N - n$ of the orbits of Zn (or O) atoms within the nth wall are given in the second, third, fourth and fifth column, respectively. In the last column a function $f_n = \sum_{m=1}^{n} N_n$, which determines the total number N of the orbits within the structure H(n_1, n_2) (by the formula $N = f_{n_2} - f_{n_1}$), is given. It is assumed that $n, n_1, n_2 = 1, 2, \ldots$, and 3H($0, n_2$) is considered to be composed of $(1, n_2)$ and d_1 orbits of the wall $n = 0$. The Kronecker delta is denoted as $\delta_{p,q}$, while δ_q^p is equal to one if q divides p, and vanishes otherwise.

NS	LGF	OT	W	SITE		N_n	$f_n(n_1, n_2)$
3xH	6	a_1	c	C_1	1	$2n - 1 - \delta_n^2$	$n^2 - [\frac{n}{2}]$
		b_1	b	C_{1v}	$..m$	$1 + 2\delta_n^2$	$n + 2[\frac{n}{2}]$
		d_1	a	C_{3v}	$3.m$	$\delta_{n,0}$	$\delta_{n_1,0}$
3yH	6	a_1	c	C_1	1	$n - 1 - [\frac{n}{3}]$	$\frac{n(n-1)}{2} - [\frac{n}{3}](n - \frac{3}{2}[\frac{n}{3}] - \frac{1}{2})$
		b_1	b	C_{1v}	$..m$	$1 + \delta_n^3$	$n + [\frac{n}{3}]$
		d_1	a	C_{3v}	$3.m$	$\delta_{n,0}$	$\delta_{n_1,0}$
6xH	8	a_1	c	C_1	1	$(1 - \delta_n^3)[\frac{n+1}{6}]$	$[\frac{n+1}{6}](n - 1 - [\frac{n}{3}] - 2[\frac{n+1}{6}])$
		b_1	b	C_{1v}	$..m$	$(1 - \delta_n^3)\delta_n^2$	$[\frac{n}{2}] - [\frac{n}{6}]$
6yH	8	a_1	c	C_1	1	$[\frac{n}{3}]$	$[\frac{n}{3}](n - \frac{3}{2}[\frac{n}{3}] - \frac{1}{2})$
		b_1	b	C_{1v}	$..m$	$(1 - \delta_n^3)$	$n - [\frac{n}{3}]$

where $\boldsymbol{T}_6^1(b_3)$ denotes a generalized translational group generated by rotations for $\pi/3$ which are followed by translations of $b_3/2$ (along the rotational axis).

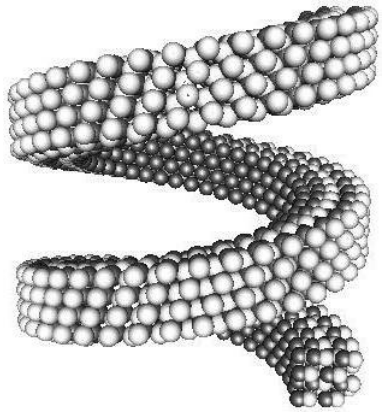

Figure 3. Nanospring $zS^{(1,1)}(4, 4)$ with radius 20 Å and helix step 30 Å.

Table 2. Nanoring orbit decompositions. For the nanoring structure specified in the first column, the line group family, orbit types (according to the notation of [19]) and the corresponding site symmetries are given in the second, third and fourth column, respectively. The total numbers of the orbits of Zn (or O) atoms within the nth wall, N_n, and in the whole nanostructure, N, are specified in the last two columns.

Nanoring	$\boldsymbol{a}_1, \boldsymbol{c}$	LG fam.	Orb. type	Site symm.	N_n	N
$zC^{a_1}cL$	$\boldsymbol{a}_1=(1,1)$ $\boldsymbol{c}=(2k+1,0)$	6	b_1	$\boldsymbol{C}_{1v}$	2	$2L$
	$\boldsymbol{a}_1=(1,1)$ $\boldsymbol{c}=(2k,0)$	6	b_1	$\boldsymbol{C}_{1v}$	1	L
			c_1	$\boldsymbol{C}_{1v}$	1	L
	$\boldsymbol{a}_1=(1,1)$ $\boldsymbol{c}=(0,n)$	3	a_2	$\boldsymbol{C}_{1h}$	1	L
			b_1	$\boldsymbol{C}_{1h}$	1	L
	$\boldsymbol{a}_1=(2,1)$ $\boldsymbol{c}=(n,0)$	7	a_1	$\boldsymbol{C}_1$	1	L
	$\boldsymbol{a}_1=(2,1)$ $\boldsymbol{c}=(0,n)$	2	a_1	$\boldsymbol{C}_1$	1	L
	Other	1	a_1	$\boldsymbol{C}_1$	2	$2L$
$xC^{a_1}cL$	$\boldsymbol{a}_1=(1,0)$ $\boldsymbol{c}=(n,0)$	8	b_1	$\boldsymbol{C}_{1v}$	1	L
	$\boldsymbol{a}_1=(1,0)$ $\boldsymbol{c}=(0,n)$	4	b_1	$\boldsymbol{C}_{1h}$	1	L
	Other	1	a_1	$\boldsymbol{C}_1$	2	$2L$

The isogonal point group is $\boldsymbol{C}_{6v}$ and it is not a subgroup of $\boldsymbol{L}_{6H}$.

Unlike the type 3H, both the nanotubes and nanowires of the type 6H consist of the same orbit types: a_1 and b_1, with stabilizers $\boldsymbol{C}_1$ and $\boldsymbol{C}_{1v}$, respectively. Hence, the site symmetry of the bulk is broken here. As for the number of orbits, the structures 6xH and 6yH differ (table 1).

Growth of ZnO nanotubes with wall thickness ∼20 nm and nanowires with diameters in the range 50–120 nm [18] and 80–150 nm [13] have been reported. Quite recently, ZnO nanotubes with an outer diameter of about 50 nm and wall thickness of 8 nm have been grown [17]. The latter would correspond to 3xH(150,178), 3yH(259,308), 6xH(448,533) or 6yH(259,308) structures. High-resolution Raman measurements with precise determination of the polarizations of the incoming and outgoing light beams are expected to distinguish between 3H and 6H structures (table 3).

2.2. Nanosprings and superlattice structured nanohelices

In contrast to the nanowires, nanotubes and nanobelts (nanoribbons) which grow along the $\boldsymbol{b}_3$ axis and thus have reduced piezoelectricity, the polar nanobelt-based structures of zinc oxide

Table 3. Piezoelectric tensor (D) components (d_{ij}), infrared and Raman active and twisting (TW) modes of ZnO nanowires and nanorings. The nanostructure is specified in the first column. $[R]$ and $\{R\}$ denote the symmetric and antisymmetric part of the Raman tensor. $\parallel$ and $\perp$ denote parallel and perpendicular polarization (relative to the nanowire/nanotube axis) of the (both incoming and outgoing) electric field vector, while $\times$ denotes crossed polarization (parallel polarization of the incoming and perpendicular polarization of the outgoing light beam or vice versa); $\parallel_\perp$ ($\times_\perp$) denotes mutually parallel (crossed) polarizations of the incoming and outgoing beam but orthogonally oriented relative to the nanowire/nanotube axis. For the nanorings we assume the order of the main axes to be greater than three.

Type	Infrared	$[R]$	$\{R\}$	TW	D
3H wire/tube	$A_0 + E_1$ $\parallel +\perp$	$2A_0 + 2E_1$ $\parallel_\perp, \parallel +\perp, \times$	$B_0 + E_1$ $\times_\perp + \times$	${}_0B_0$	$d_{14} = 0$
6H wire/tube	$A_0 + E_1$ $\parallel +\perp$	$2A_0 + E_1 + E_2$ $\parallel_\perp, \parallel + \times + \perp$	$B_0 + E_1$ $\times_\perp + \times$	${}_0B_0$	$d_{11} = d_{14} = 0$
zC^{a_1}c rings (general a_1, c)	$A_0 + A_1 + A_{-1}$ $\parallel +\perp + \perp$	$2A_0 + A_1 + A_{-1} + A_2 + A_{-2}$ $\parallel_\perp, \parallel + \times + \times + \perp + \perp$	$A_0 + A_1 + A_{-1}$ $\times_\perp + \times + \times$	${}_0A_0$	$d_{11} = 0$
$a_1 = (1, 1), (2, 1)$ $c = (n, 0)$	$A_0 + E_1$ $\parallel +\perp$	$2A_0 + E_1 + E_2$ $\parallel_\perp, \parallel + \times + \perp$	$B_0 + E_1$ $\times_\perp + \times$	${}_0B_0$	$d_{11} = d_{14} = 0$
$a_1 = (1, 1), (2, 1)$ $c = (0, n)$	$A_0^- + A_1^+ + A_{-1}^+$ $\parallel +\perp + \perp$	$2A_0^+ + A_1^- + A_{-1}^- + A_2^+ + A_{-2}^+$ $\parallel, \parallel_\perp + \times + \times + \perp + \perp$	$A_0^+ + A_1^- + A_{-1}^-$ $\times_\perp + \times + \times$	${}_0A_0^+$	$D = 0$
xC^{a_1}c rings (general a_1, c)	$A_0 + A_1 + A_{-1}$ $\parallel +\perp + \perp$	$2A_0 + A_1 + A_{-1} + A_2 + A_{-2}$ $\parallel_\perp, \parallel + \times + \times + \perp + \perp$	$A_0 + A_1 + A_{-1}$ $\times_\perp + \times + \times$	${}_0A_0$	$d_{11} = 0$
$a_1 = (1, 0)$ $c = (n, 0)$	$A_0 + E_1$ $\parallel +\perp$	$2A_0 + E_1 + E_2$ $\parallel_\perp, \parallel + \times + \perp$	$B_0 + E_1$ $\times_\perp + \times$	${}_0B_0$	$d_{11} = d_{14} = 0$
$a_1 = (1, 0)$ $c = (0, n)$	$A_0^- + A_1^+ + A_{-1}^+$ $\parallel +\perp + \perp$	$2A_0^+ + A_1^- + A_{-1}^- + A_2^+ + A_{-2}^+$ $\parallel, \parallel_\perp + \times + \times + \perp + \perp$	$A_0^+ + A_1^- + A_{-1}^-$ $\times_\perp + \times + \times$	${}_0A_0^+$	$D = 0$
Nanospring	$A_0 + A_1 + A_{-1}$ $\parallel +\perp + \perp$	$2A_0 + A_1 + A_{-1} + A_2 + A_{-2}$ $\parallel_\perp, \parallel + \times + \times + \perp + \perp$	$A_0 + A_1 + A_{-1}$ $\times_\perp + \times + \times$	${}_0A_0$	$d_{11} = 0$

(which grow along the $\boldsymbol{b}_1$-axis) are characterized by an enhanced piezoelectric effect. Namely, Kong and Wang have recently reported [20] that, by introducing dopants such as In and/or Li, the growth of free-standing nanobelts dominated by the $\pm(0001)$ polar surfaces is feasible. The nanobelts grow along $[2\bar{1}\bar{1}0]$ with the side surfaces $\pm(01\bar{1}0)$ and due to the small thickness (5–20 nm) and large aspect ratio ($\sim 1/4$) they are exceptionally flexible and tough. Therefore, the belts tend to form helical structures in order to minimize the total energy (by reducing the electrostatic but enlarging the elastic potential). As a result a right-handed nanospring of a uniform shape (width $\sim$20 nm, thickness $\sim$10 nm, radius $\sim$500–800 nm, pitch distance of 200–500 nm) is formed.

As apart from the $\pm(0001)$ polar facets, the $\pm(1\bar{2}12)$ surfaces also expose the net charge, the growth of nanosprings dominated by the latter surfaces is, in principle, possible. It should be also noted that springs are not necessarily periodic quasi-one-dimensional systems; periodic structures are characterized by the rational $Q = q/r$ values.

Nevertheless, symmetry of nanosprings is generated by the screw-axis transformation $(C_Q|f)$ (rotation of $2\pi/Q$ around the axial direction of the spring followed by a translation by f along the same axis) and can be described by first line group family [19]:

$$\boldsymbol{L}_S = \boldsymbol{T}_Q^1(f). \tag{3}$$

Equation (3) also describes the symmetry of the rigid helical structure of zinc oxide consisting of a superlattice-structured nanobelt [7] consisting of two types of alternating (polar–nonpolar) stripes whose c-axes are perpendicular to each other.

A nanospring consists of the orbits of the general (a_1) type, only. The number of orbits is determined by the number of atoms within the cross section of the nanobelt, a building block of the nanospring, as all the atoms of a nanospring sit in the general-position points of the symmetry group (3) and are characterized by the trivial stabilizer. This is very much in contrast to the situation in the bulk where all the atoms occupy special positions, being invariant under the $\boldsymbol{C}_{3v}$ point group.

2.3. Seamless nanorings

The formation of free-standing single-crystal nanorings of zinc oxide by spontaneous coaxial, uniradial and epitaxial self-coiling of a polar nanobelt has been reported quite recently [21]. The polarization across the nanobelt comes from the ionic charges on the zinc- and oxygen-terminated surfaces and the circular folding is thus driven by electrostatic interactions. The final single-crystalline structure is explained by chemical bonding between the loops.

The as-synthesized nanorings were analysed by scanning electron microscopy and high-resolution transmission electron microscopy. Typically, the nanorings dimensions are: diameter 1–4 μm, thickness 10–30 nm and shell-width 0.2–1 μm.

Two types of nanoring structure were found. The type I structure has the radial direction $[1\bar{2}10]$, tangential direction $[10\bar{1}0]$ and the nanoring axis [0001], i.e. the nanoring is made of the coiling loops of the polar nanobelt with side and top/bottom surfaces $\pm(1\bar{2}10)$ and $\pm(0001)$, respectively, and the growth direction $[10\bar{1}0]$, by interfacing the (0001) zinc and $(000\bar{1})$ oxygen planes at the same crystallographic orientation.

The structure of the type II nanoring has the radial direction $[1\bar{2}1\bar{3}]$, the tangential direction $[10\bar{1}0]$ and the nanoring plane $(1\bar{2}12)$, i.e. its building block grows along the $[10\bar{1}0]$ direction while its side and top/bottom surfaces are $\pm[1\bar{2}1\bar{3}]$ and $\pm(1\bar{2}12)$, respectively.

Although the shell-width/diameter ratio of a typical ZnO nanoring is far below the length/diameter ratio of a carbon nanotube (and many inorganic tubes as well), we shall regard nanorings (at least from the symmetry point of view) as being infinitely long, i.e. as quasi-one-dimensional crystals. The justification for such an approach can be found in the well-known

fact that a system which consists of just a few unit cells can be considered as a crystal since such an approximation would lead to an error not greater than a few per cent while it would allow one to take the benefit of introducing standard solid state concepts.

Hence, the standard notion of a chiral vector can be introduced: $\boldsymbol{c} = n_1\boldsymbol{a}_1 + n_2\boldsymbol{a}_2$, where $\boldsymbol{a}_1$ and $\boldsymbol{a}_2$ are the unit vectors of the polar nanobelt and (n_1, n_2) are the chiral indices. After the belt is self-coiled, the chiral vector reposes along the circumference of the ring. The minimal thickness of the ring $t_{\min}$ can be easily calculated by the following formula: $t_{\min} = [\boldsymbol{b}_1, \boldsymbol{b}_2, \boldsymbol{b}_3]/|\boldsymbol{a}_1 \times \boldsymbol{a}_2|$. In general, an L-walled nanoring is $L\,t_{\min}$ thick. In such a case we assume that the central wall is just folded from the layer while the inner/outer ones are proportionally shrunk/stretched. Typically, L is not a small number: a 10 nm thick nanoring actually consists of 35 layers.

In order to cut out a polar nanobelt from the bulk it should be sawn along the Zn^{2+}- and O^{2-}-terminated surfaces. In the wurtzite structure there are two classes of such surfaces and thus two family types of the polarization-induced nanorings can be imagined. However, the nanorings, grown so far, correspond to family members with maximal symmetry.

Surfaces of the first class are perpendicular to the z-axis of the bulk. Therefore, the layers to be circularly folded are parallel to the z-axis (figure 4) and they can be uniquely enumerated by the lattice vectors $\boldsymbol{a}_1 = l_1\boldsymbol{b}_1 + l_2\boldsymbol{b}_2 = (l_1, l_2)$ and denoted as zC(l_1, l_2). (Note that $\boldsymbol{a}_1$ is the minimal lattice vector in the chosen direction if l_1 and l_2 are non-negative co-primes, figure 4.) The lattice of the layer is rectangular with unit vectors $\boldsymbol{a}_1$ and $\boldsymbol{b}_3$ and the single-layer thickness is $\sqrt{3}b/2\sqrt{l_1^2 + l_2^2 - l_1l_2}$ (area of the xy-plane unit cell $\sqrt{3}b_1^2/2$ over the $\boldsymbol{a}_1$-vector length $b\sqrt{l_1^2 + l_2^2 - l_1l_2}$). In particular, the layers (1, 1) and (2, 1) have evenly distributed ($a_1/2$-spaced) mirror and glide planes, respectively. When rolled up they yield maximally symmetric rings, the very structure types that were reported to be synthesized [21]. An L-walled nanoring with chiral vector $\boldsymbol{c} = n_1(l_1\boldsymbol{b}_1 + l_2\boldsymbol{b}_2) + n_2\boldsymbol{b}_3$ we denote as zC$^{(l_1,l_2)}(n_1, n_2)L$.

The second class has charged surfaces that are parallel to the $(1\bar{2}12)$ lattice plane (figure 5), and the belt should be sawn along the x-axis (lattice vector $\boldsymbol{a}_2 = 2\boldsymbol{b}_1 + \boldsymbol{b}_2$), which is not perpendicular to the $(1\bar{2}12)$ plane. In order to define the slope we use the rectangular lattice of the cross section (periods $\boldsymbol{b}_2$ and $\boldsymbol{b}_3$) and introduce the lattice vector $\boldsymbol{a}_1 = l_1\boldsymbol{b}_2 + l_2\boldsymbol{b}_3$ which defines the sawing direction (minimal vector along the direction is obtained if l_1 and l_2 are co-primes). Therefore, the periods of the lattice to be folded, xC$^{(l_1,l_2)}$, are $\boldsymbol{a}_1$ and $\boldsymbol{a}_2$, and the rings are parameterized by the chiral vector $\boldsymbol{c} = n_1\boldsymbol{a}_1 + n_2\boldsymbol{a}_2$, figure 6. Note that although the procedures of sawing zC and xC layers are different, the layers xC$^{(0,1)}$ and zC$^{(2,1)}$ are identical. The single-loop thickness is $bb_3/2\sqrt{l_1^2b^2 + l_2^2b_3^2}$. Here also there are special choices of $\boldsymbol{a}_1$ which yield enlarged symmetry of the coiled structures: in addition to the above commented xC$^{(0,1)}$, the structure xC$^{(1,0)}$ is the single choice that matches the same conditions. Again, as the layers are invariant under the mirror reflections, the resulting rings folded along the chiral vectors $(n, 0)$ and $(0, n)$ will have vertical and horizontal mirror symmetry.

Conceptually, the method of deriving the line group symmetry of the nanorings is the same as the method used in the case of carbon nanotubes [9]. However, the details of deduction are quite different as the lattice of the polar nanobelt is rectangular in contrast to the hexagonal structure of the graphite.

The symmetry of the (n_1, n_2) nanoring can be described by the first line group family [19]:

$$\boldsymbol{L}_{\mathrm{zC}} = \boldsymbol{T}_q^r(a)\boldsymbol{C}_n, \tag{4a}$$

as it is generated by roto-helical transformations originating from the coiled lattice translations and does not depend on L (number of walls). The rotational axis order, n, is the greatest

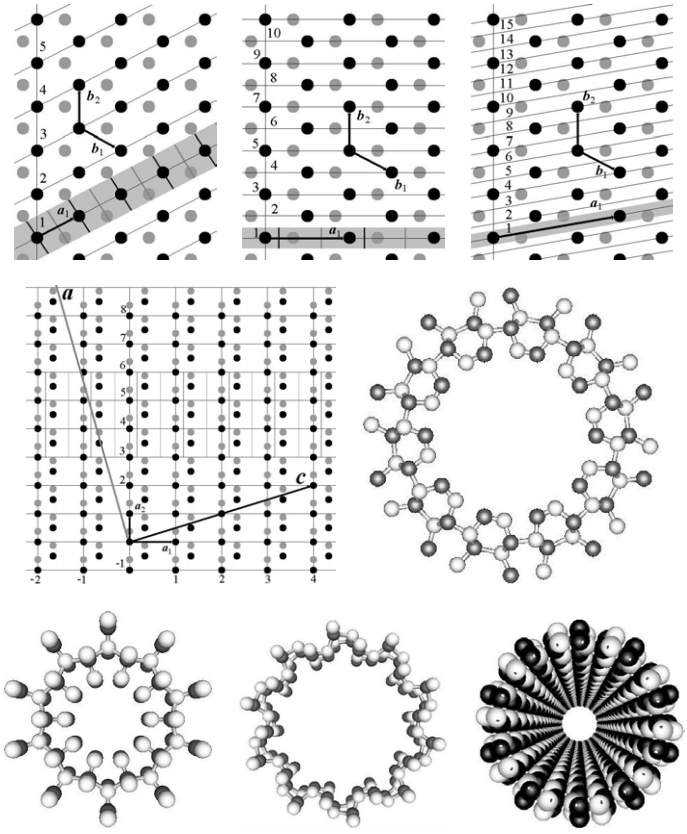

Figure 4. Upper panels: top view of zC belts, with the $\boldsymbol{a}_1$ vector being (from the left to the right): (1, 1), (2, 1) and (3, 2). Grey and black dots denote sites at $z = 0$ and $z = b_3/2$. The walls (of a coiled ring) are enumerated, and the first one is shaded. Mirror and glide planes are indicated. Central panel left: side view of the $zC^{(2,1)}$ belt. Grey and black dots denote ions of zinc and oxygen. The belt is divided, by the bold lines, into $3a_2$ wide ribbons. Within one of such ribbons the glide planes are depicted. The remaining pictures are (clockwise): $zC^{(1,1)}(0, 10)2$, $zC^{(2,1)}(0, 10)2$, $zC^{(2,1)}(10, 0)2$ and $zC^{(1,1)}(10, 0)2$ nanorings.

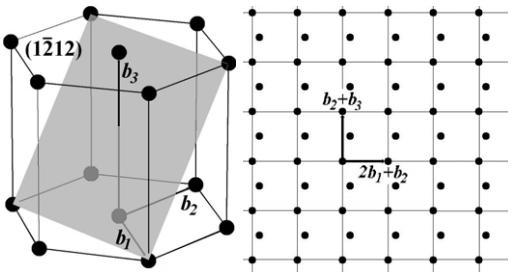

Figure 5. Structure model of the ZnO polar surface (1$\bar{2}$12).

common divisor (GCD) of the nanoring parameters, n_1 and n_2. The unit cell length a and screw-axis parameters, r, q, can be determined in the following way. First, co-primes α_1 and α_2 which satisfy the relation $\boldsymbol{a}_1^2/\boldsymbol{a}_2^2 = \alpha_1/\alpha_2$ ($\boldsymbol{a}_1$, $\boldsymbol{a}_2$ are the lattice vectors of the polar nanobelt

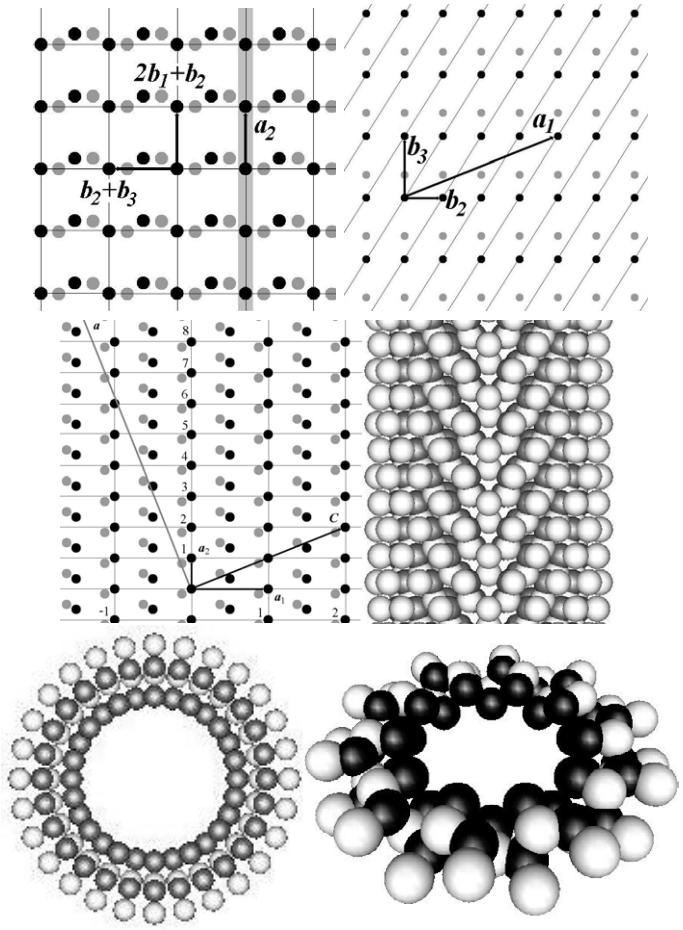

Figure 6. Upper panel, left: top view of the xC belt sawn along the $\boldsymbol{a}_2$ direction. The minimal belt of such a type is shaded. Grey and black dots depict the sites of oxygen and zinc ions within the neighbouring planes parallel to the $(1\bar{2}12)$ polar surface. Upper panel, right: plane perpendicular to $\boldsymbol{a}_2$ vector; $\boldsymbol{a}_1 = 4\boldsymbol{b}_2+\boldsymbol{b}_3$. Intersection lines with the family of crystal planes parallel with $(1\bar{2}12)$ are indicated. Central panels: side view of the $\mathrm{xC}^{(4,1)}$ belt (left) and $\mathrm{xC}^{(1,0)}(14, 0)2$ nanoring (right). Bottom panels: $\mathrm{xC}^{(1,0)}(14, 0)2$ and $\mathrm{xC}^{(1,0)}(0, 10)2$ nanorings.

and can be measured experimentally) should be defined. Then,

$$q = n\tilde{q}, \qquad \tilde{q} = \frac{1}{n^2\alpha}(\alpha_1 n_1^2 + \alpha_2 n_2^2), \tag{4b}$$

$$a = a_2\sqrt{\frac{\alpha_1}{\alpha}\tilde{q}}, \tag{4c}$$

$$r_0 = \frac{n_2\alpha_2}{n\beta_1\alpha}x + \left(\frac{n_1\alpha_1}{n\alpha}X - x\right)y\frac{\tilde{q}}{\beta_1}, \tag{4d}$$

where $\alpha = \mathrm{GCD}(\frac{n_1}{n}, \alpha_2)\mathrm{GCD}(\alpha_1, \frac{n_2}{n})$, $\beta_i = \mathrm{GCD}(\frac{n_i}{n}, \tilde{q})$; x and y are the minimal integers which satisfy $x\frac{n_1/n}{\beta_1} = 1 + X\frac{\tilde{q}}{\beta_1}$ and $\frac{n_2}{n}y = 1 + Y\beta_1$, for some integers X and Y. Parameters r_0 and $\tilde{q}$ are co-primes. Note that instead of r_0, $r_i = r_0 + i\tilde{q}$ $(i = 1, 2, \ldots)$ would yield the same line group. For convenience, by r is denoted the minimal value which is co-prime with q.

Assuming that the central wall is just folded from the layer while the inner/outer ones are proportionally shrunk/stretched, the outer diameter D of the ring is

$$D = \frac{na_2}{\pi}\sqrt{\frac{\alpha\tilde{q}}{\alpha_2}} + \frac{1}{2}Lt_{\min}.$$

The chiral angle of the nanoring is given by the formula:

$$\theta = \arcsin\left(\frac{n_1}{n}\sqrt{\frac{\alpha_1}{\alpha\tilde{q}}}\right).$$

Thus, a chiral nanoring (n_1, n_2), $0 < \theta < \pi/2$, is characterized by nontrivial helical symmetry, and quite large a and q values, (4*c*). In other words, most of the translational symmetry of the belt is transformed to the high-order screw-axis symmetry of the ring.

On the other hand, the symmetry of the zig-zag $(n, 0)$ and armchair $(0, n)$ nanorings, having, respectively, zero and right angle chirality, is parameterized by $q = n$ and $r = 1$. The helical symmetry here thus degenerates into the pure translational symmetry: $\boldsymbol{T}(a_2)$ and $\boldsymbol{T}(a_1)$, respectively. Kong *et al* [21] recently reported the nanoring structure of type I to be almost zig-zag, i.e. with a small helical angle of 0.3°.

As mentioned earlier, self-coiling of the $\mathrm{zC}^{(1,1)}$ and $\mathrm{zC}^{(2,1)}$ polar belts along the achiral directions yields rings with enlarged symmetry. To be more specific, the $\mathrm{zC}^{(1,1)}$ nanobelt, when folded along the zig-zag/armchair direction, forms a nanoring which is invariant under vertical/horizontal mirror reflection. Its symmetry group thus belongs to the sixth and third line group family [19]:

$$\boldsymbol{L}^{(1,1)}_{\mathrm{zC}\mathcal{Z}} = \boldsymbol{T}(a)\boldsymbol{C}_{nv}, \tag{5a}$$

$$\boldsymbol{L}^{(1,1)}_{\mathrm{zC}\mathcal{A}} = \boldsymbol{T}(a)\boldsymbol{C}_{nh}. \tag{5b}$$

Analogously, the glide plane symmetry of the $\mathrm{zC}^{(2,1)}$ belt is retained in the zig-zag ring structure while, in the armchair case, it becomes a roto-reflectional symmetry. The corresponding groups belong to the seventh and second line group family [19]:

$$\boldsymbol{L}^{(2,1)}_{\mathrm{zC}\mathcal{Z}} = \boldsymbol{T}_c(a)\boldsymbol{C}_n, \tag{6a}$$

$$\boldsymbol{L}^{(2,1)}_{\mathrm{zC}\mathcal{A}} = \boldsymbol{T}(a)\boldsymbol{S}_{2n}; \tag{6b}$$

where $\boldsymbol{T}_c(a)$ is a cyclic group, generated by the glide plane transformation $(\sigma_\mathrm{v}|a/2)$.

Finally, symmetry groups of the zig-zag and armchair rings obtained by coiling the belt of the type $\mathrm{xC}^{(1,0)}$ belong to the eighth and fourth line group family [19]:

$$\boldsymbol{L}^{(1,0)}_{\mathrm{xC}\mathcal{Z}} = \boldsymbol{T}^1_{2n}(a)\boldsymbol{C}_{nv}, \tag{7a}$$

$$\boldsymbol{L}^{(1,0)}_{\mathrm{xC}\mathcal{A}} = \boldsymbol{T}^1_{2n}(a)\boldsymbol{C}_{nh}, \tag{7b}$$

exactly matching the symmetries of the zig-zag and armchair single-wall transition metal dichalcogenide nanotubes [22].

The orbit decompositions of the above-listed nanoring structures are given in table 2. Also, it should be noted that the isogonal point groups of the armchair nanorings $\mathrm{zC}^{(2,1)}(0, n)$, for n odd, and $\mathrm{xC}^{(1,0)}(0, n)$, for any n, contain spatial inversion, and consequently cannot exhibit piezoelectricity.

3. Symmetry-based properties

Symmetry is essential for understanding underlying physical properties. It also enables applications of the powerful group theoretical techniques. In this section we use the presented symmetry classification of the zinc oxide nanostructures to derive some of their physical properties determined by symmetry.

3.1. Quantum numbers and band degeneracies

The quantum mechanical description of the physical processes in ZnO nanostructures is based on the conservation laws imposed by symmetry which can be expressed in terms of the good quantum numbers. Band assignation by all quantum numbers is essential for the applications of the selection rules [23] in calculations of the physical properties of the nanostructures.

The translational symmetry (with period a) is introduced by conserved quasi-momentum k taking values from the one-dimensional Brillouin zone $(-\pi/a, \pi/a]$. In the case of the armchair nanorings it can be reduced to the irreducible domain $[0, \pi/a]$ due to the horizontal mirror symmetry. Isogonal rotations are reflected in the z-component of the quasi-angular momentum quantum number m which, for nanowires and nanotubes of the 3H (6H) type, takes the values 0 and 1 (integers from the interval $[0, 3]$) as the vertical mirror symmetry makes m and $-m$ equivalent. However, as the symmetry transformations of the 6H structure form a non-symmorphic line group (2), the isogonal rotations are not necessarily the symmetries. Consequently, m is not a conserved quantity. Nevertheless it can be used at a cost of the more complicated selection rules. Alternatively, helical quantum numbers, helical momenta $\tilde{k}$ and complementary angular momenta $\tilde{m}$ can be used.

Concerning the nanosprings, usage of the $(\tilde{k}, \tilde{m})$ quantum numbers, $\tilde{k} \in (-\pi/f, -\pi/f]$, $\tilde{m} \in (-q/2, q/2]$, is indispensable as these structures are incommensurate, generally. For rational $Q = q/r$ (i.e. in the case of a commensurate structure) the period is $a = qf/n$ and quasi-momentum $k \in (-\pi/a, \pi/a)$ is conserved. As the symmetry group is Abelian, the bands are non-degenerate unless time-reversal symmetry is present.

Nanorings, nanotubes and nanowires have additional, mirror reflection symmetries, which yield parity quantum numbers and double band degeneracy (fourfold if the time-reversal is included). Also, nanorings of type II have a non-symmorphic symmetry (7*a*) or (7*b*).

3.2. Phonons, Raman and infrared active modes

While the Raman effect and infrared activity in the wurtzite-type crystals had been measured and analysed in the late 1960s [25], the pioneering works on Raman spectroscopy of hexagonal ZnO nanowires, following the discovery of the novel zinc oxide nanostructures [1], have been reported only quite recently [3, 5].

Here we give the symmetry analysis of the phonon modes of all the quasi-one-dimensional nanostructures of ZnO. Special attention is given to the Raman and infrared active modes.

Apart from the symmetry group, the classification of the normal modes of vibration depends on the orbits out of which the physical system is formed. The general classification for all orbit types of the line groups is presented in [19]. As the orbit decomposition of the ZnO nanostructures is given in the previous section, each particular classification of the phonons can be easily found.

The dynamical representations of the 3H and 6H types of the ZnO nanotubes and nanowires are:

$$D^{\mathrm{dyn}}_{3\mathrm{H}} = 2\sum_{k}\left[(3N_a + 2N_b + N_d)_k A_0 + (3N_a + N_b)_k B_0 + (6N_a + 3N_b + N_d)_k E_1\right]; \tag{8}$$

$$D^{\mathrm{dyn}}_{6\mathrm{H}} = 2\sum_{k}\left[(3N_a + 2N_b)({}_k A_0 + {}_k A_3) + (3N_a + N_b)({}_k B_0 + {}_k B_3) + 3(2N_a + N_b)({}_k E_1 + {}_k E_2)\right], \tag{9}$$

where N_a, N_b and N_d denote respectively the number of orbits of a_1, b_1 and d_1 type; ${}_k A_m$ and ${}_k B_m$ are one-dimensional (1D) irreducible representations (IRs) with even and odd, respectively, vertical mirror parity; ${}_k E_m$ are 2D IRs with no parity.

Phonons in the nanosprings and chiral nanorings are characterized by 1D IRs ${}_{\tilde{k}}A_{\tilde{m}}$ and ${}_kA_m$. (For instance, under the screw-axis transformation $(C_q|f)$ of a nanospring, they are multiplied by $\exp(\mathrm{i}\tilde{k}f + \mathrm{i}\tilde{m}2\pi/q)$.)

Dynamical representations of the nanorings with enhanced symmetry are listed below (+ and − denote, respectively, even and odd horizontal mirror parity):

$$D^{\mathrm{dyn}}_{\mathrm{zC}^{(1,1)}(n,0)} = 2L\sum_k\left[4_kA_0 + 2_kB_0 + 6\sum_{m=1}^{[n/2]}{}_kE_m + 3_kA_{n/2} + 3_kB_{n/2}\right]; \tag{10}$$

$$D^{\mathrm{dyn}}_{\mathrm{zC}^{(1,1)}(0,n)} = 2L\sum_{m=-[\frac{n-1}{2}]}^{[n/2]}\left[4_0A^+_m + 2_0A^-_m + 3_\pi A^+_m + 3_\pi A^-_m + 6\sum_k{}_kE_m\right]; \tag{11}$$

$$D^{\mathrm{dyn}}_{\mathrm{zC}^{(2,1)}(n,0)} = 6L\sum_k\left[{}_kA_0 + {}_kB_0 + {}_kA_{n/2} + {}_kB_{n/2} + 2\sum_{m=1}^{[\frac{n-1}{2}]}E_m\right]; \tag{12}$$

$$D^{\mathrm{dyn}}_{\mathrm{zC}^{(2,1)}(0,n)} = 6L\sum_{m=-[\frac{n-1}{2}]}^{[n/2]}\left[{}_0A^-_m + {}_0A^+_m + {}_\pi A^-_m + {}_\pi A^+_m + 2\sum_k{}_kE_m\right]; \tag{13}$$

$$D^{\mathrm{dyn}}_{\mathrm{xC}^{(1,0)}(n,0)} = 2L\sum_k\left[2_kA_0 +{}_k\ B_0 + 2_kA_n + {}_kB_n + 3\sum_{m=1}^{n-1}{}_kE_m\right]; \tag{14}$$

$$D^{\mathrm{dyn}}_{\mathrm{xC}^{(1,0)}(n,0)} = 2L\left[\sum_{m=1-n}^{n}\left({}_0A^-_m + 2_0A^+_m + 3\sum_k{}_kE_m\right) + 3\sum_{m=1}^{n}{}_\pi E_m\right]. \tag{15}$$

Raman active symmetric modes pertain to the all above-listed dynamical representations. They are also infrared active in all the cases except for the armchair nanorings where the infrared active modes are ${}_0A^-_0$, ${}_0A^+_1$ and ${}_0A^+_{-1}$ ($A_{2\mathrm{u}}$, $B_{2\mathrm{u}}$ and $B_{1\mathrm{g}}$ in the crystallographic notation). Nanowires, nanotubes and zig-zag nanorings, on the other hand, are also characterized by Raman active modes with ${}_0B_0$ symmetry (this changes sign under the vertical mirror reflection) and doubly degenerated infrared active phonons with ${}_0E_1$ symmetry. Armchair nanorings are, however, in contrast to all the other ZnO nanostructures, characterized by ${}_0A^-_1$, ${}_0A^-_{-1}$, ${}_0A^+_2$ and ${}_0A^+_{-2}$ Raman active modes.

A complete symmetry analysis of the Raman and infrared activity, including polarization and antisymmetric Raman tensor components, is given in table 3. Namely, in contrast to the bulk wurtzite structure [25], the antisymmetric part of the Raman tensor may be relevant for ZnO nanostructures with non-trivial helical axis [26]. It should be also noted that, due to the symmetry, the polarizability tensor of the ZnO nanostructures is diagonal with two independent components [24] (likewise the case of carbon and transition metal dichalcogenide nanotubes [9, 22]).

Our results are in accordance with the previously reported measurements of Raman scattering on aligned ZnO NWs (zinc oxide nanowires) on Si substrate [3, 5]. Namely, differences in the Raman spectra obtained by Zhang *et al* and Hsu *et al* can be explained by symmetry arguments. As listed in table 3, the A_1 TO (transversal optical) mode is active if the incident light beam is polarized perpendicularly to the NW axis, while the A_1 LO (longitudinal optical) mode can be seen if the light is polarized along the NW axis. (Note that the A_1 mode is, within the line group notation, denoted as ${}_0A_0$.) The appearance of the doubly degenerate mode in both the spectra is also consistent with our symmetry analysis, as this mode is active in crossed polarization, irrespective of the orientation of the incident beam (i.e. the incident beam being polarized parallel and the outgoing one orthogonal to the NW axis or vice versa).

3.3. Piezoelectricity

It is well known that the wurtzite crystal structure of ZnO shows piezoelectricity, i.e. that under a mechanical strain it develops a spontaneous dipole moment. This property can be described by the piezoelectric tensor, which is of the third order and symmetric with respect to the last two indices, as it relates the dipole moment (vector representation) to the strain (polar symmetric second rank tensor). As the order of the principal axis of isogonal rotation in the nanostructures (and in the bulk as well) is at least three, the general form of the piezoelectric tensor D is:

$$D_1 = \begin{pmatrix} d_{11} & 0 & d_{15} \\ 0 & -d_{11} & d_{14} \\ d_{15} & d_{14} & 0 \end{pmatrix}, \qquad D_2 = \begin{pmatrix} 0 & -d_{11} & -d_{14} \\ -d_{11} & 0 & d_{15} \\ -d_{14} & d_{15} & 0 \end{pmatrix},$$

$$D_3 = \begin{pmatrix} d_{31} & 0 & 0 \\ 0 & d_{31} & 0 \\ 0 & 0 & d_{32} \end{pmatrix},$$

where the D_i matrices actually contain D_{ijk} components (e.g., d_{11} in D_1 is in fact D_{111} and so on).

In some of the structures certain d_{ij} elements vanish due to the symmetry. For instance, in the case of a nanowire (or nanotube) of the 6H type the elements d_{11} and d_{14} vanish. The same holds for the bulk as it is characterized by the same point group. On the other hand, as mentioned in the previous section, some of the armchair nanorings exhibit no piezoelectricity whatsoever ($D = 0$). We give a detailed symmetry analysis of the piezoelectric tensor elements for various ZnO nanostructures in table 3.

4. Summary

All the geometrical symmetries of ZnO nanowires, nanotubes, nanosprings and nanorings are found and some of the symmetry based properties are derived. As these structures are quasi-one-dimensional crystals, their symmetries are described by the line groups: each of these structures has different symmetry, which on the nanoscale strongly affects their physical properties. Orbit types, conserved quantum numbers and possible band degeneracies are determined. Modes of lattice vibration are fully symmetry-assigned, Raman and infrared active modes, in particular. General forms of the piezoelectric tensor are discussed.

The most helpful technical benefit of the results presented lies in the possibility of performing extremely efficient calculations (e.g. electronic band and optical response function calculations) which are based on the modified Wigner projector method [27]. Namely, if instead of the standard elementary cell, the symmetry cell (which consists of the orbit representatives only) is used and just the relevant (irreducible) (sub)space is considered, a great efficiency can be achieved. The time-saving rate grows with the number of atoms within the unit cell and is thus directly related to the helicity order of the system considered.

Acknowledgments

This work is supported by Serbian Ministry of Science (Project No 1924), Greek–Serbian bilateral scientific project No 451-01-02501 and Pavle Savić.

References

[1] Pan Z W, Dai Z R and Wang Z L 2001 *Science* **291** 1947
[2] Wang Z L 2004 *J. Phys.: Condens. Matter* **16** R829

[3] Zhang Y, Jia H, Wang R, Chen C, Luo X, Yu D and Lee C 2003 *Appl. Phys. Lett.* **83** 4631
[4] Ng H T, Chen B, Li J, Han J, Meyyappan M, Wu J, Li S X and Haller E E 2003 *Appl. Phys. Lett.* **82** 2023
Geng B Y, Wang G Z, Jiang Z, Xie T, Sun S H, Meng G W and Zhang L D 2003 *Appl. Phys. Lett.* **82** 4791
Zhang B P, Binh N T, Segawa Y, Wakatsuki K and Usami N 2003 *Appl. Phys. Lett.* **83** 1635
Xing Y J, Xi Z H, Xue Z Q, Zhang X D and Song J H 2003 *Appl. Phys. Lett.* **83** 1689
[5] Hsu H C, Cheng C S, Chang C C, Yang S, Chang C S and Hsieh W F 2005 *Nanotechnology* **16** 297
[6] Kong Y C, Yu D P, Zhang B, Fang W and Feng S Q 2001 *Appl. Phys. Lett.* **78** 407
Park W I, Jun Y H, Jung S W and Yi G-C 2003 *Appl. Phys. Lett.* **82** 964
Zhao D, Liu Y, Shen D, Lu Y, Zhang L and Fan X 2003 *J. Appl. Phys.* **94** 5605
Hong S, Joo T, Park W I, Jun Y H and Yi G-C 2003 *Appl. Phys. Lett.* **83** 4157
[7] Gao P X, Ding Y, Mai W, Hughes W L, Lao C and Wang Z L 2005 *Science* **309** 1700
[8] White C T, Robertson D H and Mintmire J W 1993 *Phys. Rev.* B **47** 5485
[9] Damnjanović M, Milošević I, Vuković T and Sredanović R 1999 *Phys. Rev.* B **60** 2728
[10] Damnjanović M, Vuković T, Milosević I and Nikolić B 2001 *Acta Crystallogr.* A **57** 304
[11] Milošević I, Živanović R and Damnjanović M 1997 *Polymer* **38** 4445
[12] Kopsky V and Litvin D (ed) 2003 *Inernational Tables for Crystallography* vol E *Subperiodic Groups* (Dordrecht: Kluwer)
[13] Li S Y, Lee C Y and Tseng T Y 2003 *J. Cryst. Growth* **247** 357
[14] Wang R M, Xing Y J, Xu J and Yu D P 2003 *New J. Phys.* **5** 115.17
[15] Zhang Y, Jia H and Yu D 2004 *J. Phys. D: Appl. Phys.* **37** 413
[16] Yan J F, Lu Y M, Liang H W, Liu Y C, Li B H, Fan X W and Zhou J M 2005 *J. Cryst. Growth* **280** 206
[17] Wu G S, Xie T, Yuan X Y, Li Y, Yang L, Xiao Y H and Zhang L D 2005 *Solid State Commun.* **134** 485
[18] Kong X, Sun X, Li X and Li Y 2003 *Mater. Chem. Phys.* **82** 997
[19] Milošević I and Damnjanović M 1993 *Phys. Rev.* B **47** 7805
[20] Kong X Y and Wang Z L 2003 *Nano Lett.* **3** 1625
[21] Kong X Y, Ding Y, Yang R and Wang Z L 2004 *Science* **303** 1348
[22] Milošević I, Vuković T, Damnjanović M and Nikolić B 2000 *Eur. Phys. J.* B **17** 707
[23] Damnjanović M, Božović I and Božović N 1983 *J. Phys. A: Math. Gen.* **16** 3937
Damnjanović M, Božović I and Božović N 1984 *J. Phys. A: Math. Gen.* **17** 747
Damnjanović M, Božović I and Božović N 1984 *J. Phys. A: Math. Gen.* **17** 2599
Damnjanović M, Božović I and Božović N 1985 *J. Phys. A: Math. Gen.* **18** 923
[24] Milošević I 1995 *Phys. Lett.* A **204** 63
[25] Arguello C A, Rousseau D L and Porto S P S 1969 *Phys. Rev.* **181** 1351
[26] Long D A 1977 *Raman Spectroscopy* (New York: McGraw-Hill)
[27] Damnjanović M, Milošević I, Dobardžić E, Vuković T and Nikolić B 2005 *Applied Physics of Nanotubes: Fundamentals of Theory, Optics and Transport Devices* ed S V Rotkin and S Subramoney (Berlin: Springer) chapter 2, pp 41–88